NREL/TP-451-5190 • UC Category: 273 • DE93000045

Role of Polycrystallinity in CdTe and $CuInSe_2$ Photovoltaic Cells

Annual Subcontract Report 1 April 1991 – 31 March 1992

NREL/TP--451-5190

DE93 000045

J. R. Sites
Colorado State University
Fort Collins, Colorado

NREL technical monitor: B. von Roedern

National Renewable Energy Laboratory
1617 Cole Boulevard
Golden, Colorado 80401-3393
A Division of Midwest Research Institute
Operated for the U.S. Department of Energy
under Contract No. DE-AC02-83CH10093

Prepared under Subcontract No. XC-0-10046-1

November 1992

On September 16, 1991 the Solar Energy Institute was designated a national laboratory, and its name was changed to the National Renewable Energy Laboratory.

Printed in the United States of America
Available from:
National Technical Information Service
U.S. Department of Commerce
5285 Port Royal Road
Springfield, VA 22161

Price: Microfiche A01
Printed Copy A03

Codes are used for pricing all publications. The code is determined by the number of pages in the publication. Information pertaining to the pricing codes can be found in the current issue of the following publications which are generally available in most libraries: *Energy Research Abstracts (ERA)*; *Government Reports Announcements* and Index (*GRA* and I); *Scientific and Technical Abstract Reports (STAR)*; and publication NTIS-PR-360 available from NTIS at the above address.

SUMMARY

The limiting role of polycrystallinity in thin-film solar cells has been reduced somewhat during the past year, and efficiencies of both CdTe and $CuInSe_2$ cells are approaching 15%. Quantitative separation of loss mechanisms shows that individual losses, with the exception of forward recombination current, can be made comparable to their single crystal counterparts. One general manifestation of the extraneous trapping states is that the voltage of all polycrystalline thin-film cells drifts upward by 10-50 mV following the onset of illumination.

TABLE OF CONTENTS

FIGURES

TABLES

1. INTRODUCTION

Comparative quantitative analysis of individual loss mechanisms has been extended to a large number of CdTe and $CuInSe_2$ solar cells from a variety of laboratories during the past year.

A fairly detailed analysis of high-efficiency CdTe cells from nine laboratories is given in Section 2. The following section gives the results from $Cu(In,Ga)Se_2$ cells made at Boeing and CuInSe cells from the EUROCIS collaboration. Finally, Section 4 summarizes a fairly extensive study of transient voltage effects following the onset of illumination or bias voltage.

The experimental and analytical studies in this report were done in large part by research students Rick Sasala, Xiaoxiang Liu, and Ingrid Eisgruber. Much of the experimental data for Section 2 was provided by Keith Emery of NREL or taken from the open literature. CdTe cells analyzed were fabricated by Ametek Applied Materials Laboratory, Battelle Europe, British Petroleum, Georgia Tech, the Institute of Energy Conversion, Matsushita, Microchemistry, Ltd., Photon Energy, the University of Queensland, and the University of South Florida. $CuInSe_2$ cells and related came from the Boeing Company, EUROCIS, the Institute of Energy Conversion, and International Solar Energy Technology. Numerous colleagues, at both NREL and many of the laboratories above, contributed important suggestions and lively discussion of the results reported here.

2. CdTe COMPARATIVE ANALYSIS

The bandgap of CdTe (1.45 eV at room temperature) is nearly ideal for the solar spectrum. Thin-film polycrystalline CdTe has also proven to be a relatively forgiving photovoltaic material, as evidenced by the wide variety of deposition techniques that have produced solar cells with efficiencies above 10%. Until recently, however, the difference between CdTe potential and actual cells has been relatively large due to

difficulties with contacts, excessive forward recombination, bulk resistance, and window absorption. Those difficulties are now being reduced, although at different rates by different manufacturers, and CdTe cells are beginning to realize their potential. Cells from nine laboratories which are listed with assigned abbreviations in Table 2-1. In general, these are the highest efficiency cells from each laboratory that have been reported outside the laboratory. They all have a similar structure: glass, transparent conducting oxide (TCO) front contact, CdS window, CdTe absorber, and back contact.

Current-voltage, quantum efficiency, reflection, and to a lesser extent, capacitance data to quantitatively separate the individual loss mechanisms. The data used were taken from measurements in our laboratory, measurements at the National Renewable Energy Laboratory (NREL, formerly SERI), published measurements, and privately circulated data. As noted, the data in some cases were less complete or less precise than in others.

The maximum photocurrent available from a CdTe cell under the standard global spectrum[9] normalized to 100 mW/cm^2 is 30.5 mA/cm^2. Graphically, this is the area under the spectrum below the bandgap cutoff λ_g, expressed in photon current units as shown in the top half of Fig. 2-1. The bottom part of Fig. 2-1 shows the lost photon fraction, or one minus the measured quantum efficiency, as a function of wavelength for five cells. Most of the curves are normalized so that the total loss is consistent with the measured photocurrent. In two cases (QL and MC), the photocurrent was adjusted to a plausible photon-loss normalization. If one associates the different parts of this curve with the appropriate loss mechanisms, one can multiply the photon loss by the photon current, integrate, and express each loss directly in mA/cm^2.[10]

There are some similarities, and also differences, in the curves for different cells. They are all basically identical near λ_g, and the associated loss is assumed due to photons that penetrate sufficiently deep that the electron-hole pair generated is not collected. At mid-wavelengths the curves generally have a reflection loss component near 6%. Some cells had an additional relatively flat loss, which we call unidentified and suspect that it is due to metallic-like or free

Table 2-1. Recent High Efficiency CdTe Solar Cells

Manufacturer	CdTe Deposition	Highest Efficiency	Cell No.	Source of Data
University of South Florida (USF)	Close Space Sublimation	14.6%	11-4-8A	Our measurement NREL measured Ref. 1
British Petroleum (BP)	Electrodeposition	14.2%		Ref. 2,3
Photon Energy (PE)	Spray Process	12.7%	3 151 A1	NREL measured Our measurement
Microchemistry, Ltd. (MC)	Atomic Layer Epitaxy	11.5%*		Ref. 4
Matsushita (MT)	Screen Printing	11.3%		Ref. 5
University of Queensland (QL)	Electrodeposition	11.2%*		Ref. 6
Battelle Europe (BE)	Close Space Sublimation	11.0%		Ref. 7
Institute of Energy Conversion (IEC)	Physical Vapor Deposition	11.0%	40723.11-2	NREL measured
Georgia Institute of Technology (GIT)	Metal-Organic Chemical Vapor deposition	10.9%	D3	Our measurement NREL measured Ref. 8

*Current density adjusted to NREL measurement and/or quantum efficiency consistency.

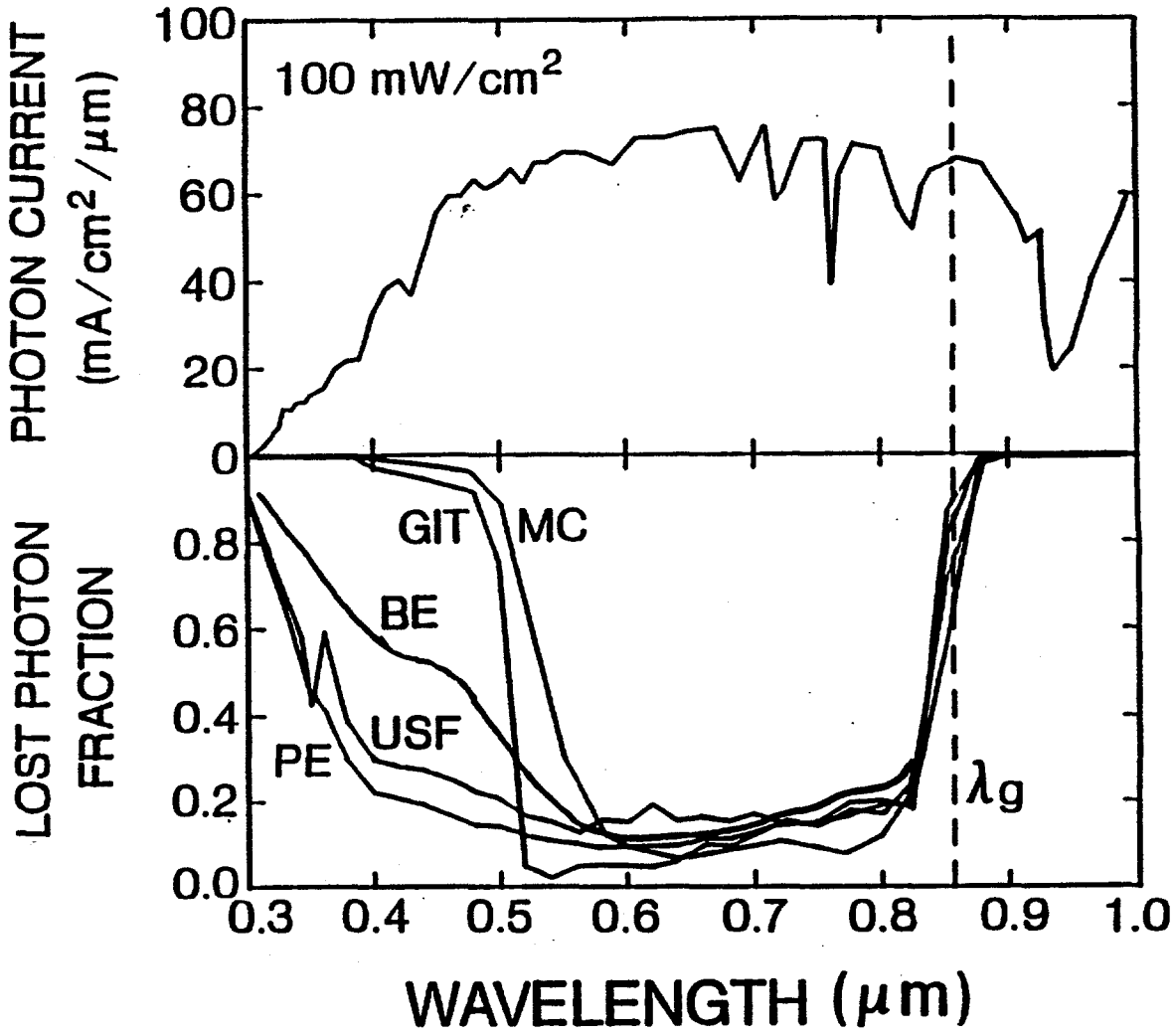

Fig. 2-1. Standard solar spectrum shown in top portion. Comparison of photocurrent losses in five cells displayed below.

electron absorption in the TCO window used. The other major loss, due to window absorption of photons with greater energy than the window bandgap, dominates the short wavelength curves. The GIT and IEC curves (IEC not shown) are what one would expect for a thick CdS window, the PE and USF curves suggest very thin CdS, and the BE curve results from an intermediate (0.1 μm) thickness. The MC window is actually more absorbing than CdS, presumably because the deliberate intermixing of CdS and CdTe to improve the junction has led to a lower bandgap window.

Fig. 2-2 gives additional information on the reflection loss, and the effect of adding a MgF_2 antireflection coating (AR) to the front surface of the glass. The measured reflection from the PE cell averages 6.5%.

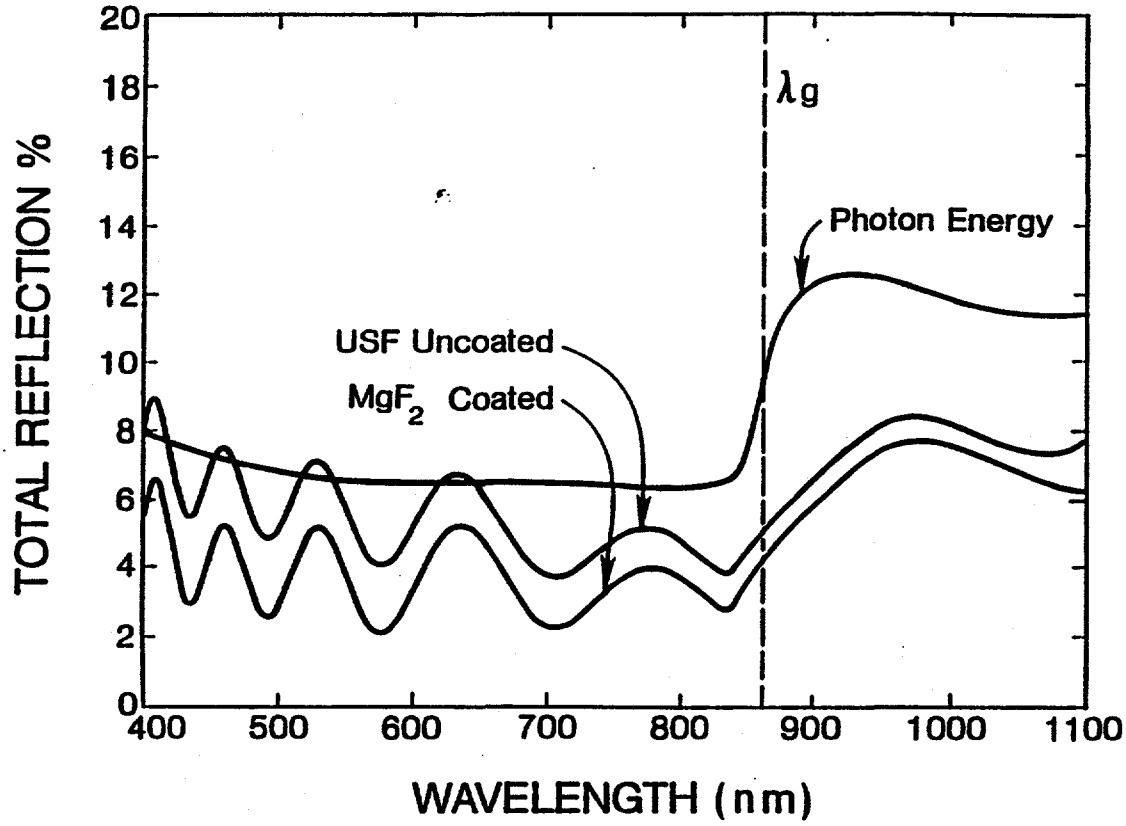

Fig. 2-2. Reflection spectrum from the Photon Energy cell and from the USF cell before and after AR coating.

The USF average reflection drops from 5.5% to just under 4% when the AR coating was added. Both cells clearly show the transition at the CdTe bandgap. The interference oscillations in the USF data, which do not change with the addition of the AR coating, are due to the smoothness of the TCO contact used.

The top section of Table 2-2 compares the photocurrent losses from the cells investigated. These are not shown for some cells because the quantum efficiency curves were not available. Also shown as a reference point for photocurrent losses and other parameters is a hypothetical 18% target cell. This column is the authors' best guess of where CdTe cells fabricated with current techniques are heading. The big variation in photocurrent loss occurs in the window. The spread of 7 mA/cm^2 in this loss is a large difference, overshadowing for example the 0.5 mA,cm^2 gain from reduced reflection with the AR coating.

Table 2-2. Comparison of Cell Parameters (100 mW/cm^2 global; 25°C)

	18% Target	USF	BP	PE	MC	MT	QL	BE	IEC	GIT
Photocurrent [mA/cm^2]	26	24.4	23.5	26.2	19.5	21.1	24.0	22.8	20.1	22.1
Photon Losses [mA/cm^2]										
Reflection	2	1.5		2	2			2	2.5	2
Window Bandgap	1.5	1		1	8			3	5.5	5.5
Deep Penetration	1	1		1.5	1			1	1.5	1
Unidentified	0	3		0	0			1.5	1	0
Open Circuit Voltage [mV]	875	850	819	790	810	797	720	750	789	745
Maximum-Power Voltage [mV]	750	686	690	585	655	634	550	599	625	588
Fill Factor [%]	79	70.5	74	61.5	73	67	65	65	69	66
Diode Quality Factor	2.0	2.6	1.9	3.6	2.2	3.0	2.7	2.8	2.75	2.8
Series Resistance [Ω-cm^2]	0	0.5	0.3	0.7	0.3	0.5	0.5	0.7	0.35	0.3
Shunt Resistance [Ω-cm^2]	∞	2000	1000	600	2400	1500	700	800	1700	800
Efficiency [%]	18	14.6	14.2	12.7	11.5	11.3	11.2	11.0	11.0	10.9

Comparison of current-voltage (J-V) characteristics is probably most usefully visualized by plotting $\log(J+J_{SC})$ vs. V. The short-circuit current density is assumed to be a reasonable approximation for the photocurrent. Fig. 2-3 shows the data for six of the CdTe cells plotted in this format. The 18% target cell, defined in Table 2-2, is used for reference. The solid symbols represent the open-circuit voltage V_{OC} and maximum power voltage V_{MP} values. Straight-line fits, representing the limit of series resistance R approaching zero and shunt resistance r approaching infinity, are determined by a technique to linearize the diode equation.[11] In the Fig. 2-3 format, a fit with a steeper and hence more desirable slope corresponds to a lower diode quality factor A. The CdTe A-factor, measured under standard illumination, is often considerably larger than that measured in the dark. The voltage difference between the lines and points from near V_{MP} upward is a consequence of series resistance effects. The current difference between points and fits at lower voltage can be due to either shunting effects or small variations of photocurrent with voltage.[12] We have not attempted here to separate the latter two effects, but instead have assumed a linear shunt resistance. The information shown graphically in Fig. 2-3 is given numerically in the lower part of Table 2-2.

The six cells included in Fig. 2-3 are separated into the top and bottom parts of the figure solely for visualization purposes. A comparison of the fits, i.e., after R and r are removed, is basically a comparison of illuminated junction quality. This comparison is commonly referred to as a voltage-response comparison, but more properly, it is a comparison of forward recombination currents which in turn determine the voltages.

Three of the cells shown (USF, BP, and MC) have quite low, and relatively similar, forward recombination currents. They can legitimately claim the best junctions. Although the USF cell has the highest V_{OC}, it also has a higher diode quality factor and consequently very similar characteristics at optimum operating voltages. In contrast, the other three cells shown (PE, QL, and GIT) have higher forward currents, and consequently their operating voltages are approximately 100 mV lower. Here also, one cell (PE) has a distinctly higher V_{OC} than the other two, but exhibits a markedly higher A-factor as well. Of the three cells not included in Fig. 2-3, the BE curve is

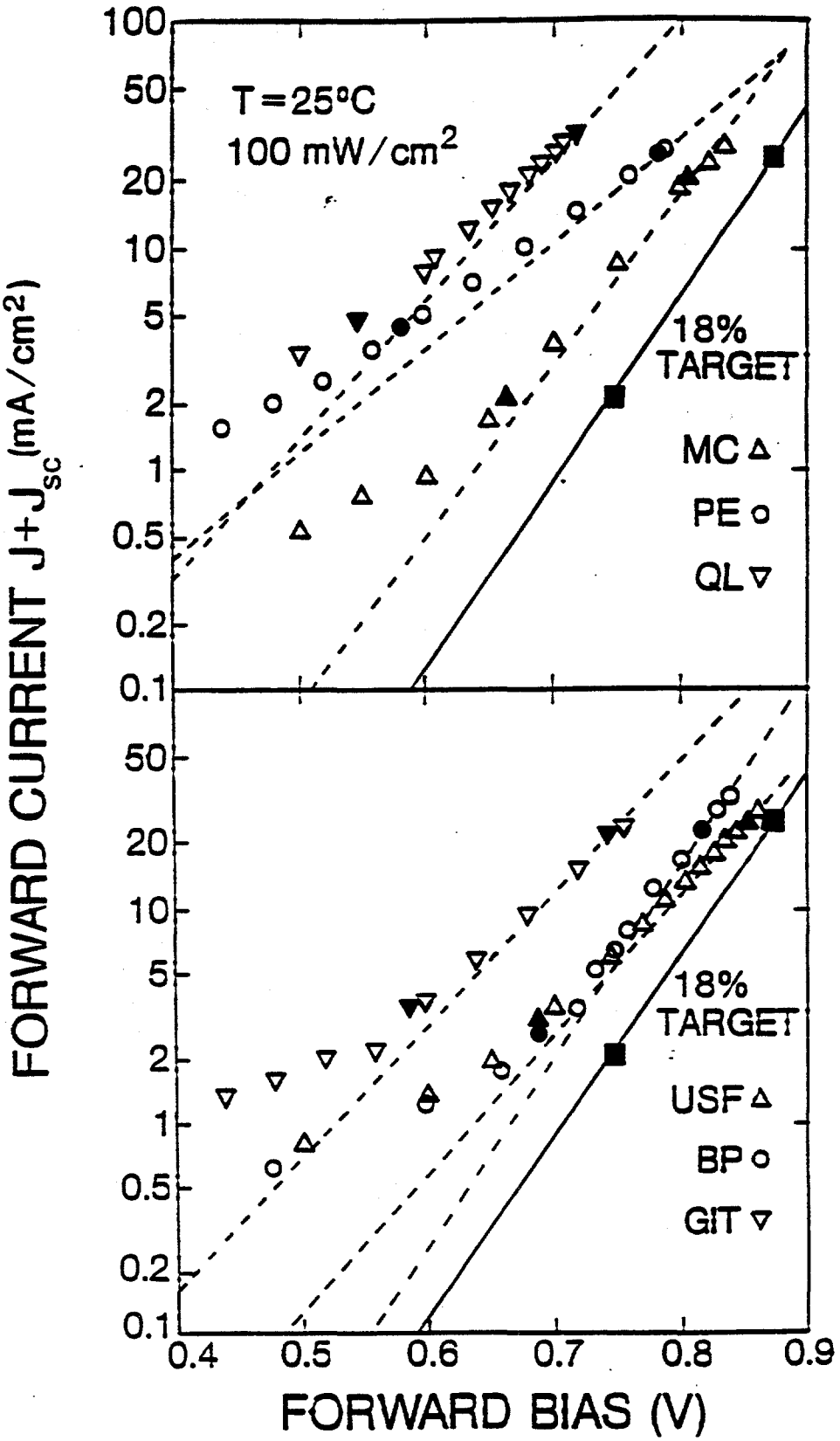

Fig. 2-3. Comparison of CdTe junctions in the light. 18% target is cell defined in Table 2-2. Straight line fits are for R = 0, r = ∞.

very similar to GIT and QL, while the IEC and MT junction properties are intermediate between the high and low forward current groups.

The series resistances of all cells listed in Table 2-2 are respectable; none exceeds 1 Ω-cm^2. The excess current at low voltages, due at least in part to shunting, is a little more of a problem, and in some cases its effect on efficiency approaches 1%.

The capacitance of a photodiode is basically a measure of its depletion width, complicated in some cases by frequency dependent trapping effects. The higher efficiency CdTe cells discussed here do not appear to have major frequency-dependent effects, at least in reverse bias, and their capacitance is relatively insensitive to illumination level.

Capacitance data from the USF cell and PE cell 151A are shown in Fig. 2-4 in the C^{-2} vs. V format. The reverse bias slope is inversely

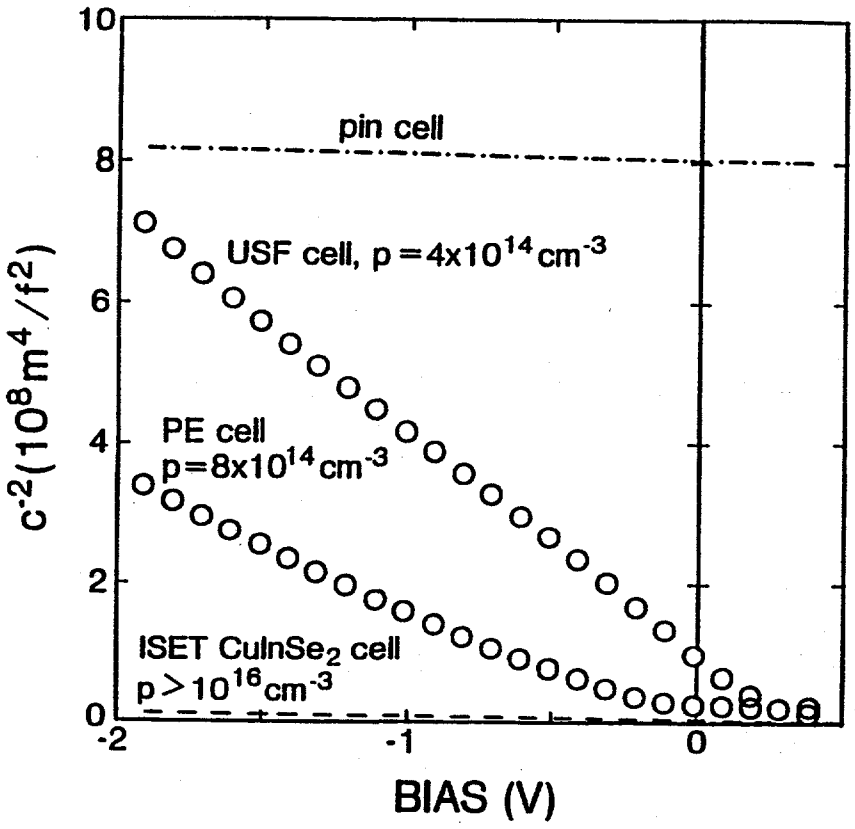

Fig. 2-4. Comparison of USF, PE and p-i-n CdTe capacitances, as well as a typical $CuInSe_2$ curve.

proportional to the hole density p. The value of the hole density is quite small, almost certainly indicating a heavy degree of compensation resulting from extraneous states in the bandgap. Published data on the other PE cell[13] and on the BP cell[3] indicate somewhat higher hole densities (low 10^{15} cm^{-3} range). In contrast, many CdTe cells studied earlier have very little voltage dependence in their capacitance, suggesting an insulating layer equal in thickness to the CdTe. These cells are appropriately labeled as p-i-n structures, and one such curve is shown for reference.

Compared to $CuInSe_2$ cells, typified by the dashed line in Fig. 2-4, all of the CdTe cells analyzed to date have very low hole densities. Because these values are so small, it is probably unrealistic to expect a correlation between hole density and V_{OC} or A-factor as has been reported for $CuInSe_2$.[14]

Table 2-3 compares the individual loss mechanisms of each cell in units of percentage reduction of efficiency compared to the 18% target. It is for the most part a reformulation of Table 2-2. In a few cases, an individual parameter has actually exceeded the target value, and those comparisons are indicated with parentheses. For the three cells where quantum efficiency curves were not available, the entire photon loss is designated as unidentified.

As suggested above, some cells, notably MC, have large photon losses due to window absorption. Others, e.g., QL, start with low values for V_{OC}. One of those listed (PE), and a large number studied previously, has a substantial loss due to a very high diode quality factor.

The efficiency losses in Table 2-3 can be divided into those that are peripheral to the diode junction (photon losses, series and shunt resistance) and those that are integral to it (V_{OC} and A-factor). The identification of the three best junction cells in the discussion of Fig. 2-3 above is in fact equivalent to summing the V_{OC} and diode quality factor losses in Table 2-3. Again, one finds that the USF, BP, and MC junctions are superior to the others and quite similar to each other. Note that they were fabricated by three different processes. At

Table 2-3. Individual Efficiency Losses Relative to 18% Target

	USF	BP	PE	MC	MT	QL	BE	IEC	GIT	Best Composite
Efficiency Achieved [%]	14.6	14.2	12.7	11.5	11.3	11.2	11.0	11.0	10.9	17.8
Efficiency Losses [%]										
Reflection	(0.3)		0	0			0	0.3	0	(0.3)
Window Bandgap	(0.3)		(0.3)	4.5			1.2	2.6	2.6	(0.3)
Deep Penetration	0		0.2	0			0	0.3	0	0
Unidentified Photon	1.7	1.7	0	0	3.0	1.4	1.0	0.5	0	0
Low V_{OC}	0.5	1.2	1.7	1.3	1.6	3.2	2.5	1.7	2.4	0.5
Diode Quality Factor	0.9	(0.1)	2.4	0.3	1.5	1.1	1.2	1.1	1.2	(0.1)
Series Resistance Effect	0.4	0.2	0.4	0.2	0.3	0.3	0.4	0.2	0.2	0.2
Shunting, $J_L(V)$ Effect	0.5	0.8	0.9	0.2	0.3	0.8	0.7	0.3	0.7	0.2
Target Efficiency [%]	18.0	18.0	18.0	18.0	18.0	18.0	18.0	18.0	18.0	18.0

this point, it would be premature to conclude that any specific fabrication process is likely to yield the best junction.

An interesting, and technologically relevant, question is whether the losses in Table 2-3 are independent. If they are, it follows that current technology should be able to combine the processes that give the smallest loss in each category. The right-most column in Table 2-3 gives the numerical result: a composite cell with 17.8% efficiency. The losses, however, may have some physical interdependence, and statistical uncertainties in the individual losses bias the composite loss on the low side. Nevertheless, it is probably correct to say that the capability for a 17% CdTe cell exists with today's technology.

3. $CuInSe_2$ PROGRESS

Major progress in the efficiency of $CuInSe_2$ solar cells [and $CuIn(Se,S)_2$] has been made by the EUROCIS collaboration.[15] The individual photocurrent losses for the highest efficiency (14.8%) cell are deduced from Fig. 3-1, which has the same format as Fig. 2-1. The analogous curve for the previous high-efficiency cell, made by ARCO is shown for comparison. The numerical losses are given in Table 3-1. There is a rough tradeoff in that the ARCO cell has very low window absorption, while the EUROCIS cell is very good at collecting the near-IR photons. The latter effect is probably due to a longer diffusion length.

The comparison of forward currents between the EUROCIS and ARCO cells under illumination is shown in Fig. 3-2. Also shown is ISET cell 489 with a very good junction, but excessive current loss. The lower forward current of the EUROCIS cell means that it has a higher voltage both at open circuit and in the operating range. At lower voltages, it suffers somewhat due to excessive shunting. Both it and the ISET cell have a good diode quality factor (1.5) and series resistance ($0.25\ \Omega\text{-cm}^2$).

The Boeing group has continued to make contributions to $Cu(In,GA)Se_2$ cells. Fig. 3-3 shows the light and dark forward currents from cell 1490. The absorber bandgap of 1.1 eV, determined from quantum efficiency measurements is about 50 meV less than many of the Boeing

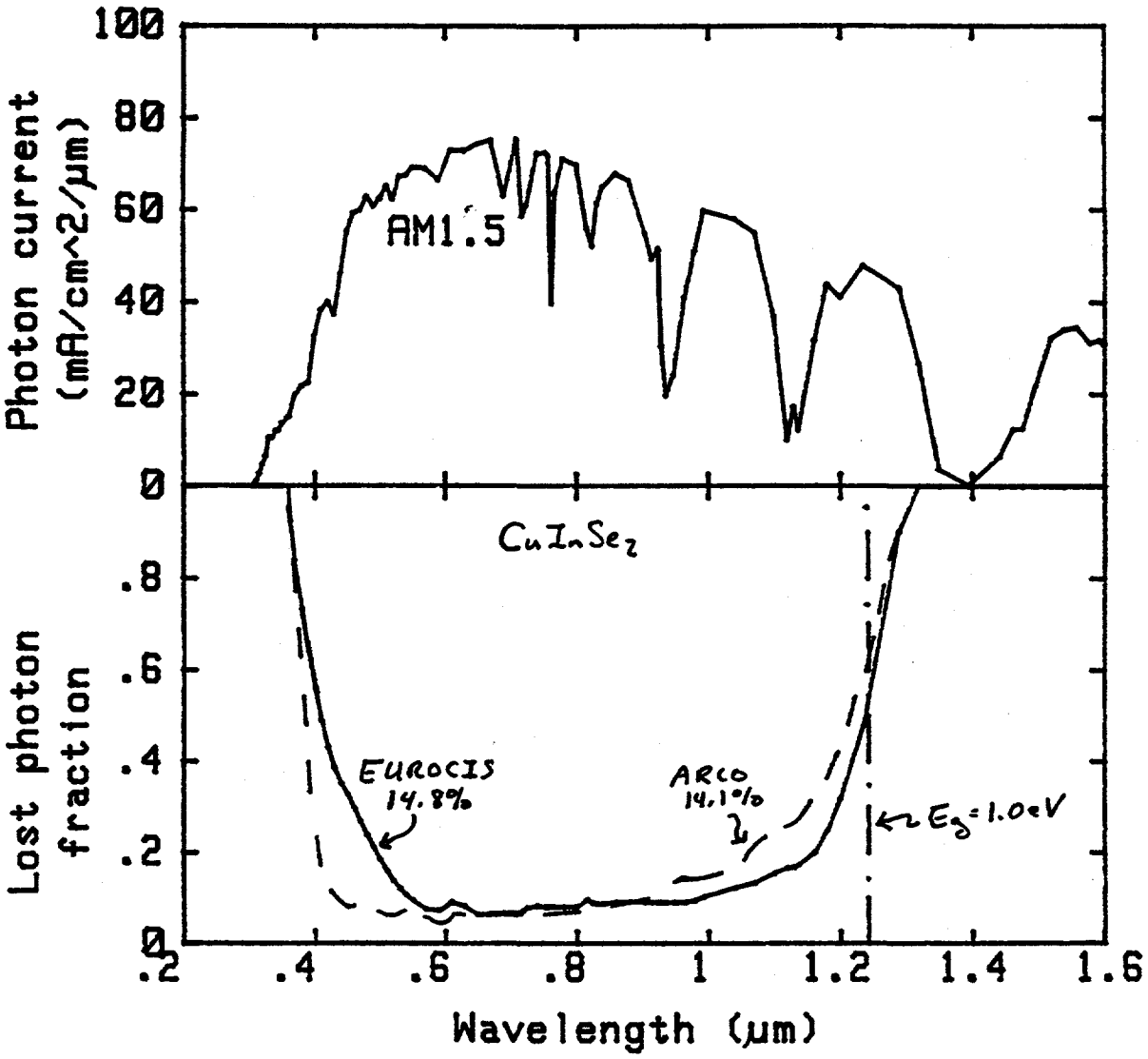

Fig. 3-1. Comparison of photon losses between highest efficiency EUROCIS and ARCO cells.

cells, but about 100 meV greater than pure $CuInSe_2$ cells. The diode quality factor (1.5) and series resistance (0.25 Ω-cm^2) are the same as the EUROCIS and ISET cells and its shunting is less than the EUROCIS cell. Consequently, its fill factor (73%) is quite high. Its voltage is slightly above the best pure $CuInSe_2$ cells, but with the higher bandgap, its potential current density is reduced by about 4 mA/cm^2. Actual current density (35 mA/cm^2) is another 9 mA/cm^2 below its potential, a slightly larger difference than that seen with the ARCO and EUROCIS cells.

Table 3-1. Photocurrent Losses from Fig. 3-1

	ARCO (14.1%)	EUROCIS (14.8%)
Photocurrent	41 mA/cm^2	40½ mA/cm^2
Reflection Loss	1	2½
Window Loss	2½	2½
Deep Penetration Loss	3½	2½
Maximum Allowed	48 mA/cm^2	48 mA/cm^2

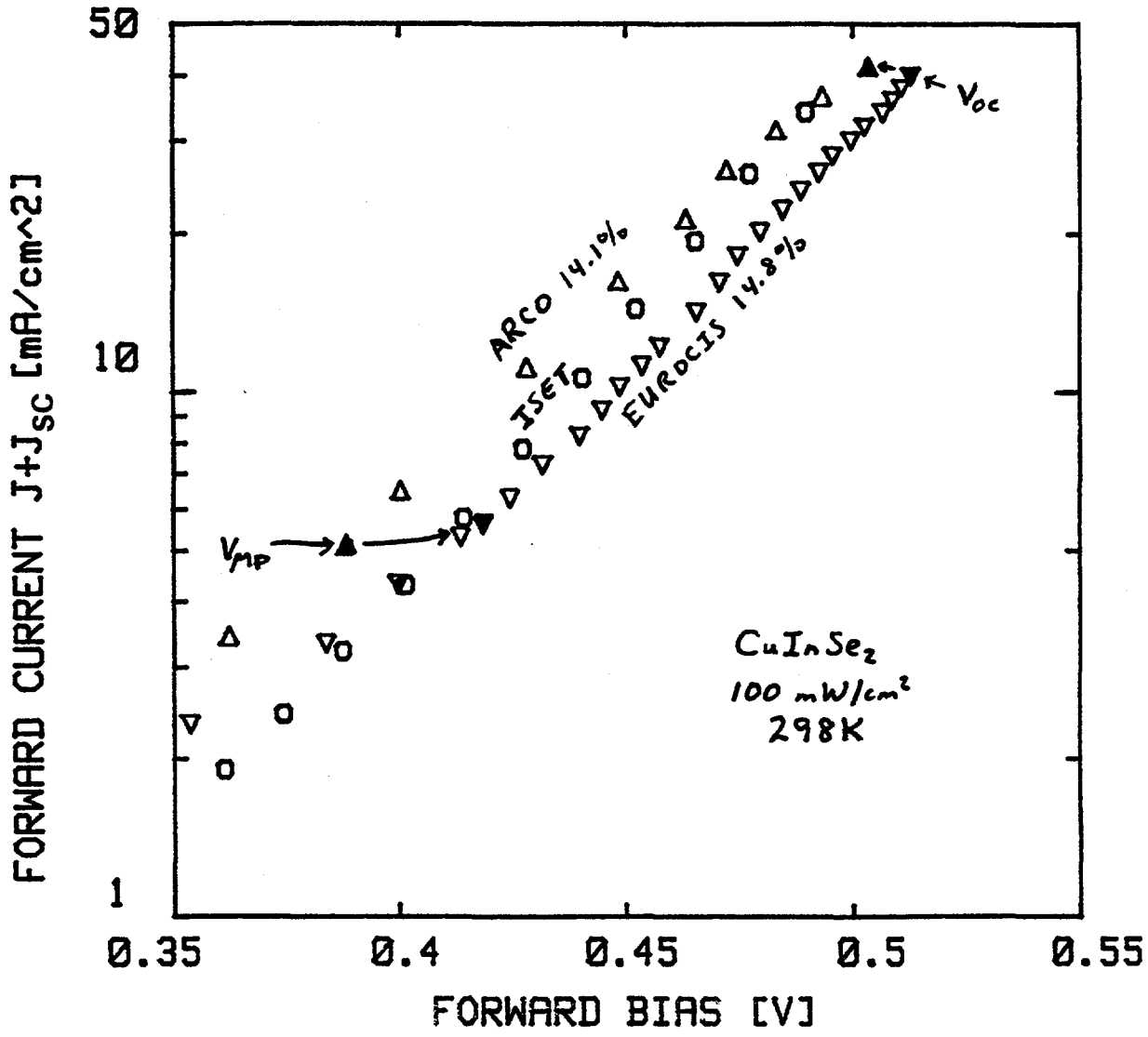

Fig. 3-2. Comparison of forward currents from $CuInSe_2$ cells with high-quality junctions.

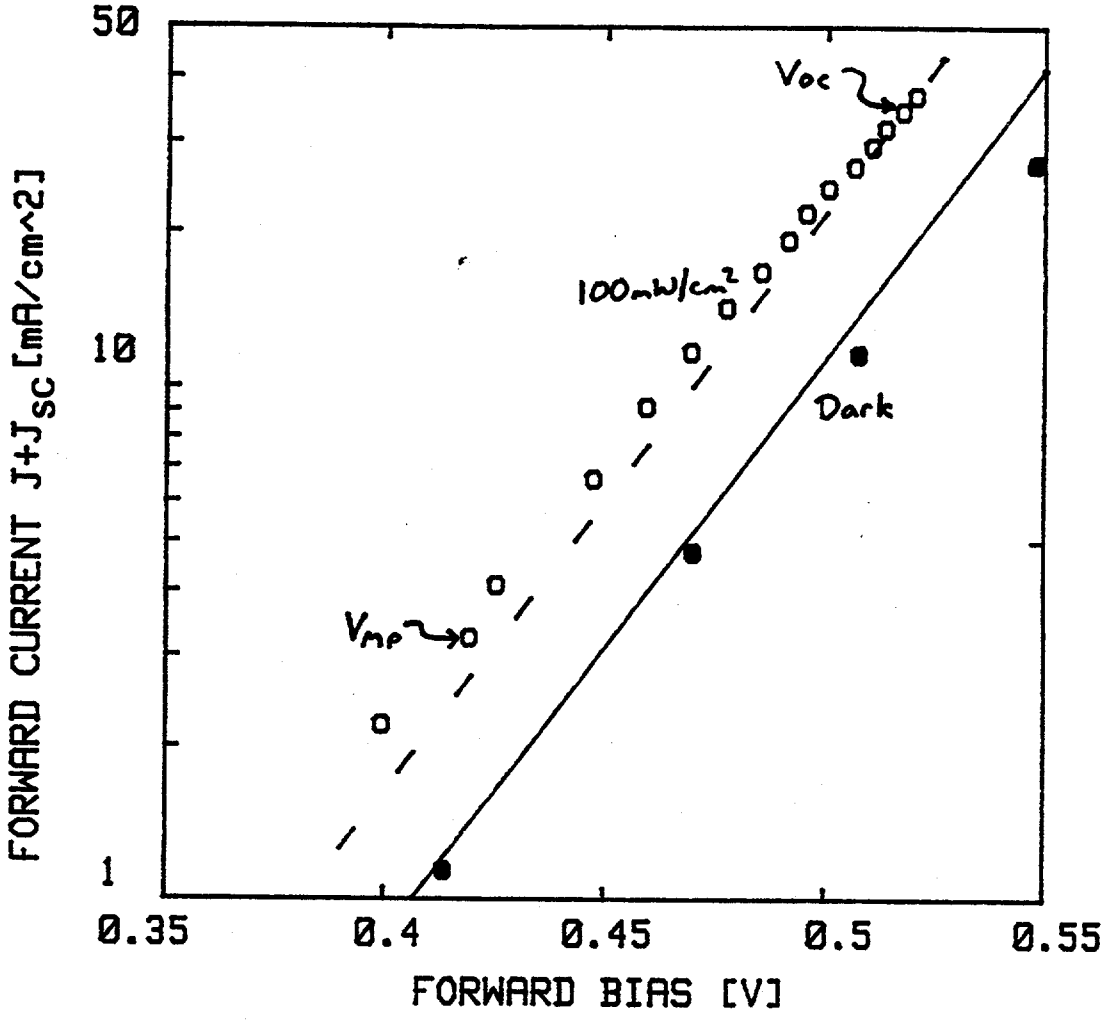

Fig. 3-3. Light and dark forward currents for Boeing Cu(In,Ga)Se_2 cell 1490 (Eg = 1.1 eV, η = 13.1%).

4. VOLTAGE TRANSIENTS

One complication with determining the efficiency of solar cells is that the voltage does not come instantaneously to its steady-state value, but continues to increase for time spans from milliseconds to minutes after exposure to light.[16-19] This effect will be referred to as the transient voltage effect and labeled ΔV. ΔV ranges between 10 and 50 mV, is qualitatively the same for both $CuInSe_2$ and CdTe, and corresponds to an incremental increase of efficiency on the order of 0.5%.

The experimental set-up is shown schematically in Fig. 4-1. Light from an ELH bulb is collimated and passed through a 35-mm camera before

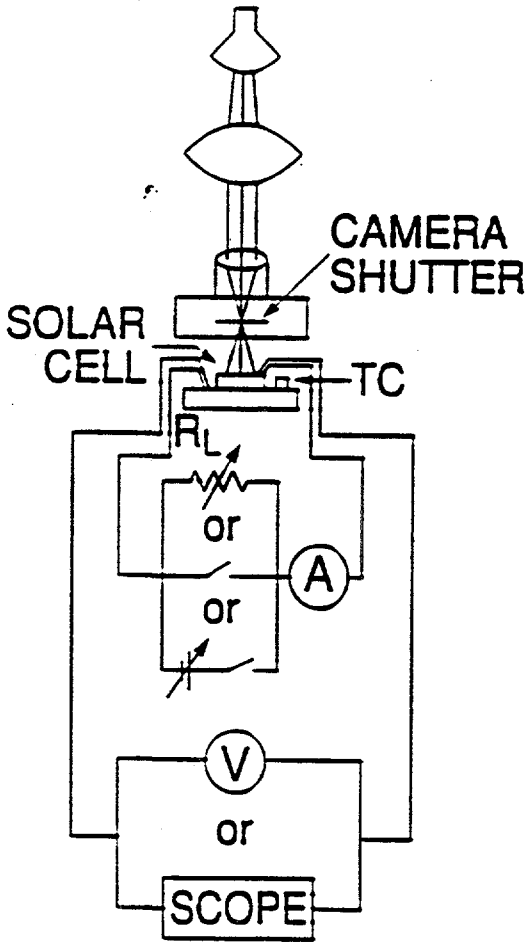

Fig. 4-1. Schematic diagram of apparatus used to measure transient voltage.

reaching the cell. the characteristic opening time for the camera shutter is less than 0.5 ms. The cell is contacted with kelvin probes to eliminate contact resistance problems. A Hewlett-Packard 54501A 100 MHz digitizing oscilloscope is used to record voltage over time ranges of 0.5 ms to 10 ms and 10 ms to 2 s. Several trials are recorded, allowing sufficient time between trials for the cell to equilibrate, and are averaged to reduce the noise level. Then the voltage, current, and thermocouple voltage are recorded with a Hewlett-Packard computer for the time range 2 to 1500 s using Keithly multi-meters and the computer's internal clock. The thermocouple is places as close as possible to the cell being tested. The temperature is stabilized by flowing cold N_2 gas under the cell or by heating it

with an infrared heater. It is crucial to control and know the temperature of the sample since voltage shifts of a few millivolts are to be measured. The temperature fluctuations are held to within ±1°C for most situations, and all data is corrected for these fluctuations.

The apparatus depicted in Fig. 4-1 allows for several different initial or final conditions: (1) The camera shutter is used for switching from initial dark to light conditions. (2) A mechanical switch provides a rapid change (≈0.5 ms) between short- and open-circuit conditions. (3) A variable bias allows adjustment of initial voltage. (4) A variable load resistor allows the study of voltage transients near maximum power or anywhere else in the cells operating range. In each case, depending on the time range, either the oscilloscope or voltmeter is connected to the cell.

Fig. 4-2 shows the transient voltage effect for a typical 9% efficient ISET $CuInSe_2$ cell which was made by the selenization method. Prior to the measurement the cell was in the dark with no applied bias. the data shown spans 0.5 ms to 1500 s following the opening of the shutter. Tests done on other ISET $CuInSe_2$ samples showed similar behavior in magnitude and form. the voltage increase continues for several decades of time, implying a continuous range of time constants from at least 10^{-4} to 10^4 s. ΔV ranges from 20 ± 3 mV for 350 K to 33 ± 3 mV for 275 K. The time that the cell requires to return to its initial state is approximately the same as the time in forward bias. In contrast to Fig. 4-2, V_{OC} for single crystal silicon solar cells varied less than 2 mV over the same range of time at each of the four temperatures used.

Most of ΔV occurs at times longer than those characteristic of a pulse simulator. Thus, pulse-simulators will record voltages lower than those under illuminated steady-state conditions. The 350 K curve saturates at about 100 s and the 325 K curve saturates at approximately 1000 s. One might expect, therefore, that the 298 K and 275 K curves saturate in the 10^4 and 10^5 s range. If one assumes that the steady-state value of dV/dT is nearly constant for times longer than the saturation time, then the 298 K curve should increase by an additional 4 mV before saturation and the 275 K curve by 17 mV.

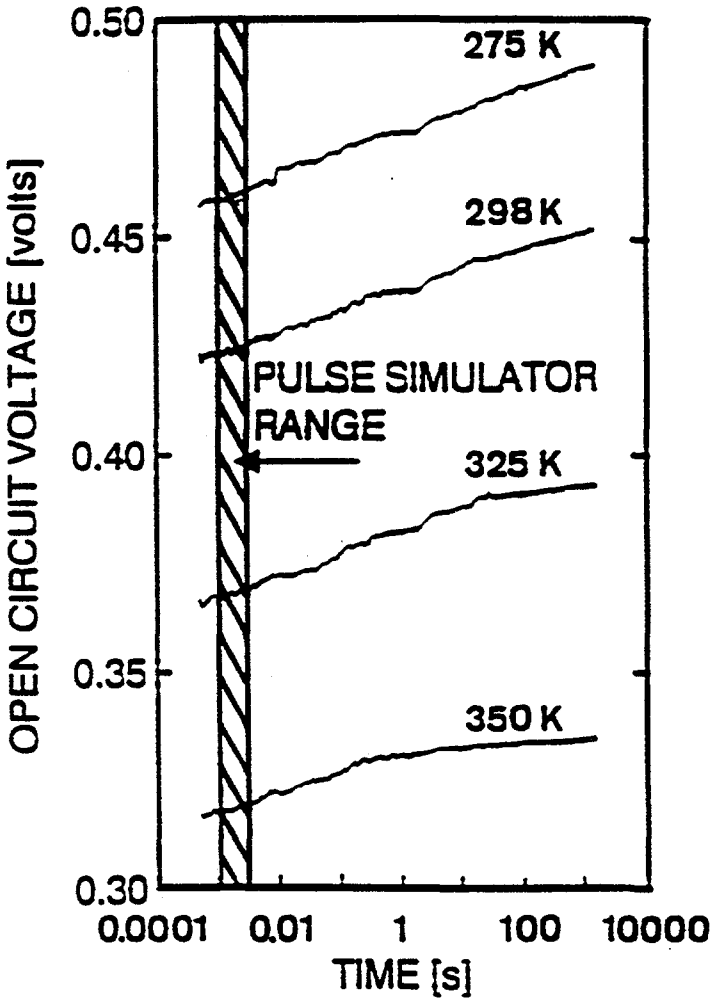

Fig. 4-2. V_{OC} transients for a typical ISET $CuInSe_2$ solar cell.

An obvious question is whether the transient voltage effect is due to the change in illumination or the change in voltage between dark and light conditions. Fig. 4-3 compares the approach to steady-state in two cases: (1) light is turned on (shutter); (2) circuit is opened (switch) after the light has been on for some time. For short times there is a difference of almost 10 mV between the data taken using the switch and shutter, but as expected the curves converge at longer times. A similar difference is seen in other cells, but usually the initial separation is less than 10 mV. The conclusion is that the transient voltage effect is primarily driven by the voltage history, rather than the illumination history, of the cell.

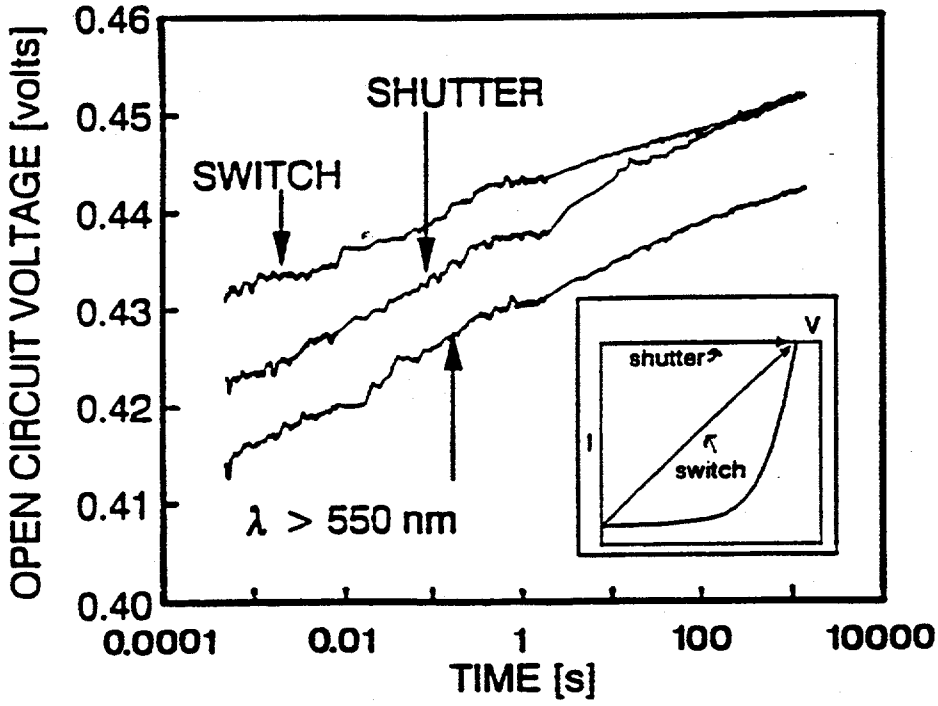

Fig. 4-3. Comparison of data taken using a switch or shutter. Also shown is voltage transient when sort wavelengths are excluded. T = 300 K.

Also shown in Fig. 4-3 is ΔV when a filter is used to block light below 550 nm. This cutoff excludes photons with sufficient energy to generate electron-hole pairs in the CdS window layer. Prior to the measurement, the cell was shorted while being soaked in the longer wavelength light which was approximately 75 mW/cm^2 in intensity. The reduction in voltage of roughly 10 mV is consistent with the lower intensity and no significant change is seen in the transient voltage effect.

Further evidence that the transient voltage effect is due to the voltage history is found in Fig. 4-4, which shows curves for the ISET cell and an evaporated IEC cell that were both held at a bias near V_{OC} in the dark for over an hour before the measurement. Also shown for reference are curves when the cells were shorted prior to the measurement. The light was turned on, the circuit quickly opened (<1 s) and the voltage was monitored as a function of time. The ISET cell was held at V_{in} = 500 mV prior to the measurement so that the voltage actually decreases slightly before equilibrating. The steady-state voltage is about 2-3 mV

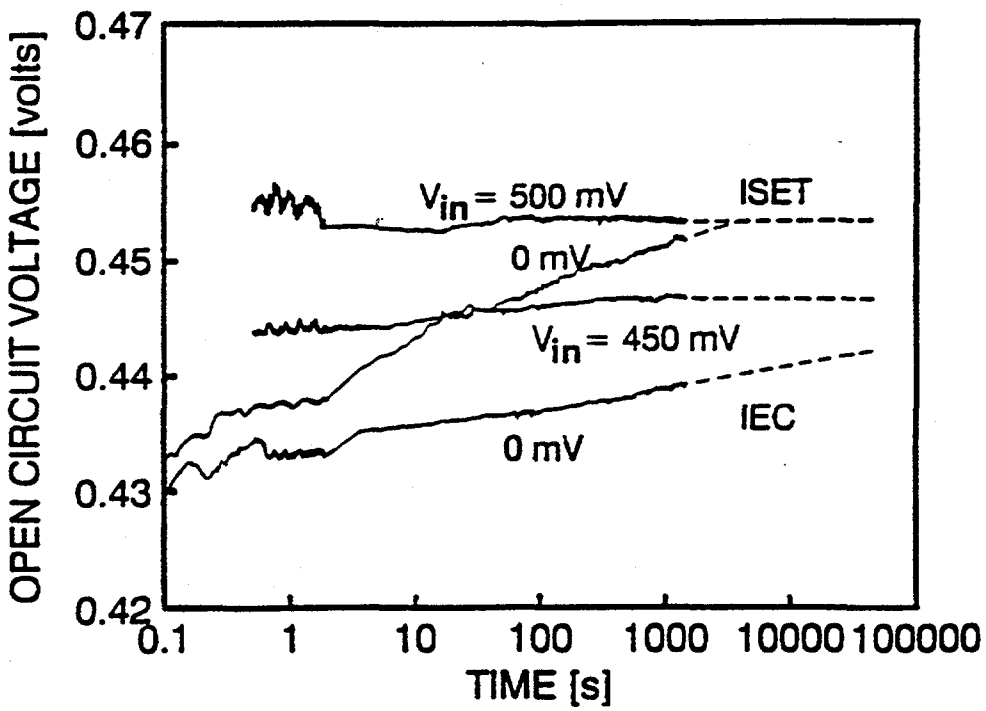

Fig. 4-4. Comparison at zero or near-V_{OC} bias for $CuInSe_2$ cells that were held in the dark prior to measurement.

higher than the highest value of the zero initial bias curve, suggesting that the curve had not yet saturated. When the ISET cell was held in the dark at biases slightly below the steady-state V_{OC}, V_{OC} did increase but saturated much more quickly than with no prior bias applied.

The IEC V_{OC} shown in Fig. 4-4 is seen to increase even after being held at 450 mV for two hours in the dark, suggesting either the effect is not solely a voltage effect for the IEC cell or that the IEC cell is slower to respond than the ISET cell. The IEC cell does saturate near 450 mV which can be taken as the steady-state V_{OC} for the cell at 298 K.

Another important issue is the nature of the transient effect at operating voltages. To investigate this question, a load resistor R_L is put in series with the cell. The measured voltages for R_L = 10 and 20 Ω-cm^2, with the cell switched from shorted to loaded under constant illumination, are shown in Fig. 4-5. The voltage shift ΔV_{CL} is slightly smaller than ΔV for R_L = 20 Ω-cm^2 near V_{MP} and much smaller than ΔV when R_L = 10 Ω-cm^2 below V_{MP}. However, the constant-current shift ΔV_{CC} is

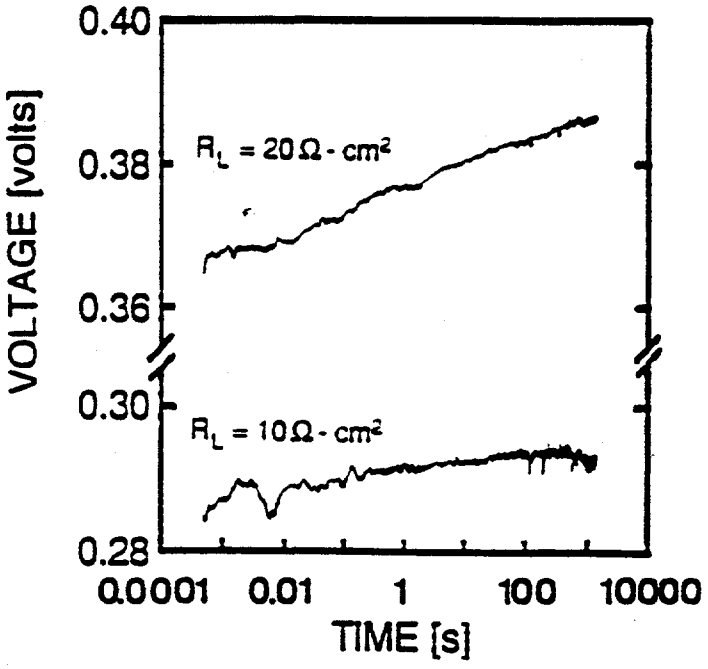

Fig. 4-5. Voltage transients for ISET $CuInSe_2$ cells with load resistor R.

very similar to ΔV at V_{OC}. The relationship between ΔV_{CC} and ΔV_{CL} is given by

$$\Delta V_{CC} = \Delta V_{CL}[1 - (J/V)/(dJ/dV)] \quad .$$

The correction in brackets is calculated form the steady-state J-V curve for the ISET cell. Multiplying the measured ΔV_{CL} by this correction factor yields $\Delta V_{CC} \approx 25$ mV for each of the three designated loads. There is, however, considerable uncertainty when $R_L \leq 10\ \Omega\text{-cm}^2$. The conclusion is that the voltage shift is similar in magnitude at V_{OC} and normal operating voltages, that is $\Delta V_{CC} = \Delta V$.

Fig. 4-6 displays the transient voltage effect seen for the IEC cell discussed above. Like the ISET cell, the dominant ΔV effect occurs over times longer than those used in pulse-simulator measurements. In this case, the voltage did not saturate at any of the temperatures used. The cell was tested at 350 K for 5000 s and still showed no clear trend of saturating. Thus it is unlikely to reach steady-state in terrestrial applications. The apparent magnitude of ΔV, ranging from 10 to 15 mV for the IEC cell, is less than the ISET cell, but the difference is

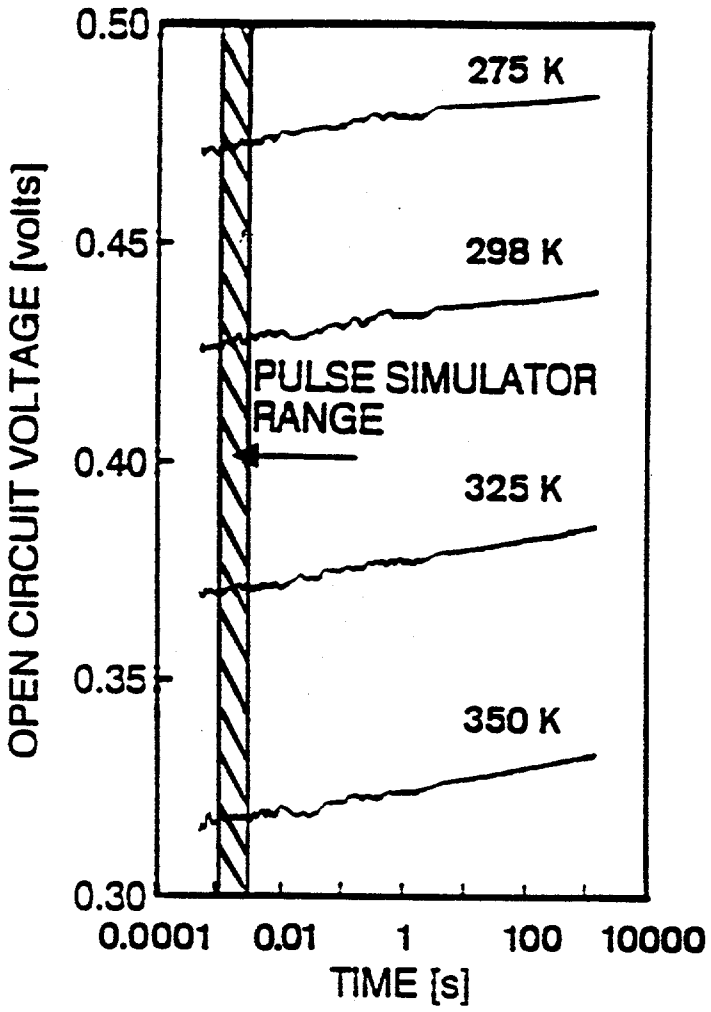

Fig. 4-6. V_{OC} transients for a typical IEC $CuInSe_2$ solar cell.

primarily due to the slower response of the IEC cell. Using the saturation value of $V_{OC} \approx 450$ mV from Fig. 4-4 as the steady-state open-circuit voltage, ΔV at 298 K will be near 25 mV, which is about the same as the ISET ΔV. When a load resistor is used with the IEC cell, the results are very similar to the ISET load resistor data.

Time dependent voltage measurements were done on several CdTe cells made by a spray process at Photon Energy Inc. The results are qualitatively the same as for the $CuInSe_2$ and are shown in Fig. 4-7 for a representative sample. The magnitude of ΔV, ranging from 30 to 40 mV, is somewhat larger than that seen with most $CuInSe_2$ cells. The CdTe cells saturate on a time scale intermediate between that of the ISET and IEC cells. Again the transient voltage effect disappears when the cells

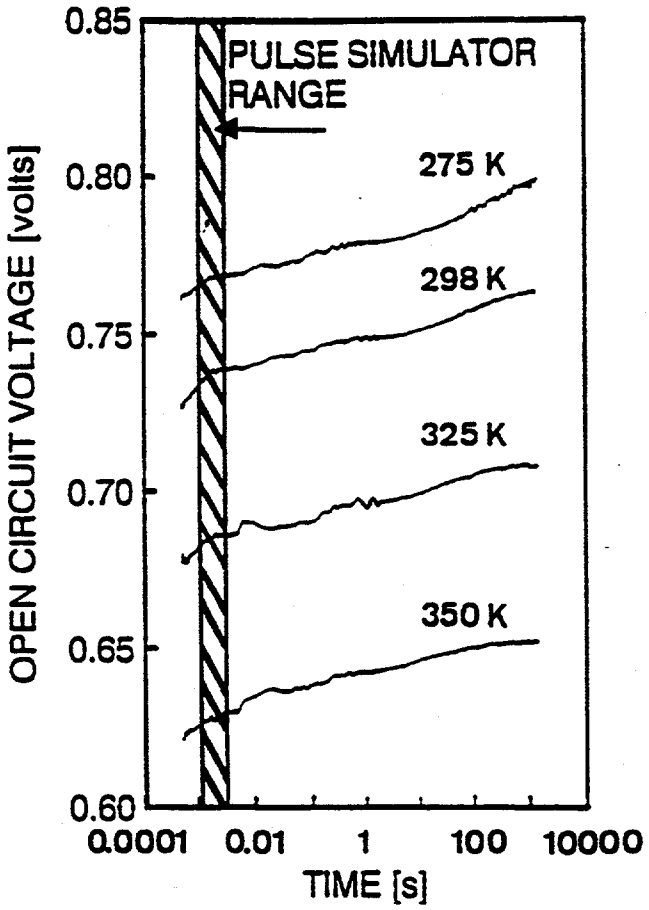

Fig. 4-7. V_{OC} transients for a typical Photon Energy CdTe solar cell.

are forward biased near the steady-state V_{OC}, and the response with a load resistor is similar to $CuInSe_2$.

In summary, after thin-film $CuInSe_2$ and CdTe solar cells are changed from zero bias to forward bias, the J-V curve continues to shift by 10-50 mV towards higher voltages. Primary observations are summarized in Table 4-1. the transient voltage effect is predominately due to the voltage history of the cell and not the illumination history. The effect is qualitatively the same for all the cells tested. However, the magnitude of ΔV and the response time of cells varies from sample to sample. It is expected that the transient voltage effect will diminish as the quality of cells improves.

An initial hypothesis for the mechanism of the transient voltage effect is that there are mid-gap traps in the $CuInSe_2$ near the junction that

Table 4-1. Summary of Transient Voltage Effect Observations

(1)	In $CuInSe_2$ and CdTe cells, magnitude is 10-50 mV and not strongly temperature dependent (in single crystal Si < 2 mV).
(2)	Effect is primarily driven by the voltage history of the cell.
(3)	Saturation time is 10^2 to 10^4 s and shorter at higher temperatures.
(4)	Time constants are continuous and span several decades, from 10^{-4} to 10^4 s.
(5)	Effect reversed when initial voltage is above steady-state V_{OC}.
(6)	Recovery time is similar to saturation time.
(7)	Effect is not driven by photons with energy above window bandgap.
(8)	Effect at operating voltage is similar to that at V_{OC}.

are filled as the cell is forward biased. The filled traps are responsible for a voltage dependent increase in the built-in potential, which results in the observed shift of voltage.

The implication of the transient voltage effect for pulse-simulator measurements is that conventional techniques will not give a precise calibration of cell or module performance. The efficiency is underestimated by roughly 0.5%. The most practical solution in general is to forward bias the module prior to the measurement and to sweep the J-V curve from higher to lower voltages to prevent relaxation while a cell is shorted. In either case, good temperature control is necessary.

5. RECOMMENDATIONS

We continue to recommend systematic and quantitative analysis of solar cell loss mechanisms. It is important for all cell manufacturers to know in some detail what is working well and where the problems lie. We especially recommend routine extraction of series and shunt resistance under illumination, since they can vary significantly among similar cells and can unnecessarily complicate the analysis of more intrinsic parameters.

For CdTe, the obvious recommendation is to explore whether the junctions produced by the University of South Florida, British Petroleum, and Microchemistry, Ltd., can be combined with the low window absorption achieved by Photon Energy while keeping the series resistance low. Similarly, with $CuInSe_2$, the question is whether the window achieved by ARCO and the high shunting resistance achieved by several groups can be integrated with the EUROCIS junction properties.

For the voltage transients, we suspect that the issue may diminish in magnitude as cell quality improves. In the meantime, since modules will probably continue to be characterized with pulse-simulators, we recommend that the modules at least occasionally be biased near V_{MP} for significant time prior to measurement. Periodic comparison of results with and without the pre-bias should offer a first order correction to routine module characterization.

6. COMMUNICATIONS

6.1. Publications

1. "Junction Analysis of Selenized $CuInSe_2$ Solar Cells," Proc. 22nd IEEE Photovoltaics Specialists Conf., p. 930 (1991). X. X. Liu, R. A. Sasala, and J. R. Sites.

2. "Comparative Analysis of Recent High-Energy CdTe Solar Cells," Journal of Solar Energy, in press. R. A. Sasala, X. X. Liu, and J. R. Sites.

3. "Transient Voltage of Thin-Film Polycrystalline Solar Cells," Am. Inst. Phys. Conf. Series, in press. R. A. Sasala and J. R. Sites.

6.2. Talks

1.	Solar Energy Research Institute	August 15, 1991
2.	PVSC21, Las Vegas	November 9, 1991
3.	Colorado Seed Growers, Estes Park, CO	December 6, 1991
4.	Colorado State University	January 21, 1992
5.	Colorado School of Mines	April 14, 1992

6.3. Specific Cell Reports

Date	Cells	Sent to
August 12, 1991	BP and USF CdTe	Ullal
August 20, 1990	USF 5-16-8-1	Zweibel
September 3/10, 1991	Photon Energy 952	Zweibel
November 15/21/27, 1991	USF 11-4-8A	Ullal
January 10, 1992	Boeing 1460AA	Ullal
February 24, 1992	SCI A749A #15	Ullal
April 8, 1992	Boeing 1490	Ullal
April 15, 1992	EUROCIS	Ullal

7. REFERENCES

1. T. L. Chu, Shirley S. Chu, J. Britt, C. Ferekides, C. Wang, C. Q. Wu, and H. S. Ullal, IEEE Trans. Electr. Dev., to be published.

2. A. K. Turner, J. M. Woodcock, M. E. Ozsan, J. G. Summers, J. Barker, S. Binns, K. Buchanan, C. Chai, S. Dennison, R. Hart, D. Johnson, R. Marshall, S. Oktik, M. Patterson, R. Perks, S. Roberts, M. Sadeghi, J. Sherborne, J. Szubert, and S. Webster, Proc. Int. PVSEC-5, p. 761 (1991).

3. J. M. Woodcock, A. K. Turner, M. E. Özsan, and J. G. Summers, IEEE PVSC 22, 842 (1991).

4. J. Skarp, Y. Koskinen, S. Lindfors, A. Rautiainen, and T. Suntola, 10th Proc. European PV Conf. (1991).

5. N. Suyama, T. Ariata, Y. Nishiyama, N. Ueno, S. Kitamura, and M. Murozono, IEEE PVSC 21, 498 (1990).

6. G. C. Morris, P. G. Tanner, and A. Tottszer, IEEE PVSC 21, 575 (1990).

7. D. Bonnet, B. Henrichs, and H. Richter, IEEE PVSC 22, 1165 (1991).

8. A. Rohatgi, S. A. Ringel, R. Sudharsanan, and H. C. Chou, IEEE PVSC 22, 962 (1991).

9. R. Hulstrom, R. Bird, and C. Riordan, Solar Cells 15, 365 (1985).

10. J. R. Sites, H. Tavakolian, and R. A. Sasala, Solar Cells 29, 39 (1990).

11. J. R. Sites and P. H. Mauk, Solar Cells 27, 411 (1989).

12. D. A. Fardig and J. E. Phillips, IEEE PVSC 22, 1146 (1991).

13. R. K. Ahrenkiel, B. M. Keyes, L. Wang, and S. P. Albright, IEEE PVSC 22, 940 (1991).

14. X. X. Liu, R. A. Sasala, and J. R. Sites, IEEE PVSC 22, 930 (1991).

15. H. Schock et al., Am. Inst. Phys. Conf. Proc. (1992).

16. M. N. Ruberto and A. Rothwarf, J. Appl. Phys. 61, 4662 (1987).

17. S. P. Albright, B. Ackerman, and R. R. Chamberlin, Photon Energy Ann. Report to NREL (1991).

18. S. Bhattacharya, G. R. Kumar, and V. Kumar, IEEE PVSC 20, 560 (1988).

19. J. M. Ruiz and M. Cid, Proc. 9th PSEC (1989), p. 690.

Document Control Page	1. NREL Report No. NREL/TP-451-5190	2. NTIS Accession No. DE93000045	3. Recipient's Accession No.

4. Title and Subtitle

Role of Polycrystallinity in CdTe and $CuInSe_2$ Photovoltaic Cells

5. Publication Date
November 1992

6.

7. Author(s)
J. R. Sites

8. Performing Organization Rept. No.

9. Performing Organization Name and Address

Department of Physics
Colorado State University
Fort Collins, Colorado 80523

10. Project/Task/Work Unit No.
PV241101

11. Contract (C) or Grant (G) No.

(C) XC-0-10046-1

(G)

12. Sponsoring Organization Name and Address
National Renewable Energy Laboratory
1617 Cole Blvd.
Golden, CO 80401-3393

13. Type of Report & Period Covered

Technical Report
1 April 1991 - 31 March 1992

14.

15. Supplementary Notes
NREL technical monitor: B. von Roedern

16. Abstract (Limit: 200 words)

This report describes work by Colorado State University (CSU) to perform comparative quantitative analyses of individual loss mechanisms for a large number of CdTe and $CuInSe_2$ solar cells from a variety of laboratories. The limiting role of polycrystallinity in thin-film solar cells has been reduced somewhat during the past year, and efficiencies of both CdTe and $CuInSe_2$ cells are approaching 15%. A quantitative separation of loss mechanisms shows that individual losses, with the exception of forward recombination current, can be made comparable to their single-crystal counterparts. One general manifestation of the extraneous trapping states is that the voltage of all polycrystalline thin-film cells drifts upward by 10-50 mV following the onset of illumination.

17. Document Analysis
a. Descriptors
cadmium telluride ; copper indium diselenide ; polycrystalline ; thin films ; photovoltaics ; solar cells

b. Identifiers/Open-Ended Terms

c. UC Categories
273

18. Availability Statement
National Technical Information Service
U.S. Department of Commerce
5285 Port Royal Road
Springfield, VA 22161

19. No. of Pages
34

20. Price
A03

Form No. 0069E (6-30-87)